EM models for evaluating rain perturbation on the NRCS of the sea surface observed near nadir

F. Capolino
L. Facheris
D. Giuli
F. Sottili

Indexing terms: Rain perturbation, Normalised radar cross section, Sea surface, EM models, Wind effects

Abstract: The authors address the problem of evaluating the normalised radar cross section (NRCS) of the sea surface perturbed by the joint effect of rain and wind, when observed close to nadir. They present a model, based on the full wave theory, for evaluating such an NRCS when varying polarisation, frequency and incidence angle (not far from nadir) for different values of wind velocity and of the root mean square height of the corrugation induced by rainfall. Some comparisons are made with the integral equation model results in the case of rain-induced corrugation alone. The two models are found to be in good agreement. In addition, partial comparisons made with experimental data suggest that the proposed model is well grounded and exploitable for application. It is indeed expected that the model can be exploited to improve precipitation measurements over the sea through spaceborne rain radar and to improve wind measurements using scatterometers in the presence of rain.

1 Introduction

Signals backscattered by the sea depend on several physical phenomena, but mainly on wind- and rainfall-induced corrugation. While the influence of wind on sea normalised radar cross section (NRCS) has been investigated in depth, the effects of rainfall are not yet well known. However, it has been shown they are not negligible [1]. Therefore, in principle, given a suitable analytical model (possibly taking advantage of specific experimental results) to represent changes of the NRCS of the water surface under the effect of rainfall, rainfall intensity could just be retrieved by measuring the sea NRCS. Furthermore, as shown in the companion paper [2], such a model can be exploited to improve the estimate of vertical profiles of rainfall rate through spaceborne weather radar.

IEE Proceedings online no. 19981901

Paper first received 11th August 1997 and in revised form 12th January 1998

The authors are with the Dipartimento di Ingegneria Elettronica, Università di Firenze, Via di Santa Marta, 3, 50139 Firenze, Italy

Raindrops falling on a water surface generate cavities with a crown, that collapse forming a vertical stalk of water, which subsides to spawn rings of gravity–capillary waves that propagate outward [3, 4]. Analysis of radar data provides evidence that the ring-waves are the dominant feature contributing to the backscattered power for incidence angles not far from nadir [1, 4], while at grazing angles stalks are the dominant feature [3]. Though the case of nadir incidence is of particular interest for spaceborne weather radars, very few results are available in the literature about the influence of rainfall rate on the power backscattered by the water surface; in particular, some results have been published on the relationship between rainfall rate and the statistic parameters of the water surface [1, 5].

In this paper, we present the application of an electromagnetic (EM) model for computing the sea surface NRCS, with the main purpose of pointing out the effects of rainfall when such a surface is jointly corrugated by wind. We limit our analysis to incidence angles not too far from nadir, accounting only for the distributed ring-waves phenomenon. Due to the total lack of experimental data referring to the third case, we proceed by analysing separately the three different cases of: (*a*) rainfall only, (*b*) wind only, (*c*) wind plus rainfall. Thus, we first refer to experimental results obtained through artificial rain [1] and derive a plausible relationship between rainfall rate and surface roughness variance. Next, to predict the NRCS in case (*a*), we use the full wave model (FWM) [6, 7] and the experimentally derived sea roughness frequency spectrum reported in [5]. Then, we check consistency of FWM predictions with experimental data in case (*b*). Finally, theoretical FWM results are presented for case (*c*) at K_u band.

Though the FWM has attracted some controversy in the past [8–11], the formulation adopted here [6, 7] was found in agreement with the integral equation model (IEM) theory [12–14] and with some experimental results. The purpose of this paper is not a validation of the FWM, but the formulation of a model able to predict satisfactorily the sea NRCS for a wide range of wind velocities and rainfall rates. In Sections 4 and 5.1 FWM is shown to provide accurate results when these two phenomena act separately. Section 4 deals with case (*a*); for cross-validation purposes we compare the FWM NRCS with the IEM NRCS at both C and K_u bands when varying incidence angle, polarisation and root mean square (rms) height of the sea surface, obtaining excellent agreement, in particular for low

incidence angles. Incidentally, a comparison between FWM and IEM has never before been presented for a two-dimensional azimuth symmetric rough surface. In Section 5.1, good agreement between FWM results and experimental data by Schroeder *et al.* [15] is shown for case (*b*). As mentioned above, in case (*c*), no comparison was possible with experimental data reported in the literature, however the FWM was found particularly suitable for sea NRCS prediction under the effect of these two statistically independent effects. Indeed, as shown in Section 5, the conditions that corrugated surfaces must meet to be implemented in a unified manner through the FWM according to [7], are largely satisfied.

2 Physical characterisation of the water surface corrugated by rainfall only

In this Section we describe the solution adopted for water surface modelling in the presence of rainfall only, allowing us to relate both the rms height and the spatial wave spectrum of the sea surface to rainfall rate.

2.1 Surface roughness height distribution

Water surface roughness is modelled through a zero mean Gaussian height distribution, with variance $\langle h^2 \rangle$. An approximate relationship between $\langle h^2 \rangle$ and rainfall rate is obtained referring to experimental results carried out with artificial rain [1]. In such experiments, a fixed raindrop size (2.8mm diameter) was used with drops falling from 1m above the water surface, thus hitting the water surface with a velocity (4.4m/s) lower than the terminal velocity of real rain. Through linear regression applied to those results (see Table 1 in [1]), we derived the following relationship between rainfall intensity (mm/h) and height variance (mm^2):

$$\langle h^2 \rangle = 11.6 \times 10^{-3} R' \qquad (1)$$

where R' is the rainfall rate of that experiment.

Our goal is to extrapolate such results to derive an analogous relationship for drops falling at their terminal velocity. As a consequence of the precipitation process, ring-waves are generated by transfer of some fraction η of the kinetic energy of the falling raindrops. We assumed that the same fraction η is transferred to generate the ring-wave phenomenon also when raindrops fall with their terminal velocity, and have different diameters. Thus, the same energy transfer for the generation of ring-waves (and the same $\langle h^2 \rangle$) corresponds to different equivalent rainfall rates, depending on the kind of rainfall. We used this assumption to determine expressions, similar to eqn. 1, for the two 'natural' rainfall cases (a) and (b) that follow.

In the experiment of [1], each raindrop contributed to the total energy with a kinetic energy $E_k = (1/2)mw^2 = 1.113 \times 10^{-4}$ J, where m is the mass of the drop (kg) and w is its impact velocity. The water volume fallen over a 1m^2 area was $V = 10^6 R'$ mm^3/h. Hence, the number of drops fallen per hour was $N_d(2.8) = V/V_d(2.8) \cong 8.7 \times 10^4 R'$, where V_d is the raindrop volume. Accordingly, the total kinetic energy reaching the unit area per hour was $E_{tot} = N_d(2.8) \cdot (1/2) \cdot m \cdot w^2 = 9.679R'$. Using eqn. 1 we get

$$E_{tot} = 835.9\langle h^2 \rangle \qquad (2)$$

and, as implicitly suggested in [1], eqn. 2 is assumed independent of the type of rainfall and drop size distribution (DSD). Let us consider now two types of DSD:

(*a*) Dirac delta-shaped DSD centred on 2.1mm (roughly the average value of real DSDs [1]). In this case, each drop falls at terminal velocity $w_t = 6.73$m/s (obtained using the Atlas formula: $w_t(D) = 9.65 - 10.3\exp(-0.6D)$ m/s [16]); its kinetic energy is the same as that of a 2.8mm diameter raindrop, but carries a different water content. Repeating the above computations, we get $N_d(2.1) = V/V_d(2.1) \cong 2.06 \times 10^5 R$, with R in mm/h. The total kinetic energy per unit area and per hour is now

$$E_{tot} = N_d(2.1)\frac{1}{2}mw_t^2 = 22.96R \qquad (3)$$

From eqns. 2 and 3 we get the relationship between the rms height $h(rms)$ in mm and R, plotted in Fig. 1

$$h(rms) = 0.166\sqrt{R} \qquad (4)$$

(*b*) Marshall–Palmer DSD, namely $N(D) = N_0 \cdot \exp(-\Lambda D)$ with $\Lambda = 4.1R^{-0.21}$, $N_0 = 8 \times 10^3$m^3/mm and D in mm [16]. The total kinetic energy for drops at terminal velocity is

$$E_{tot} = 3.6\frac{\pi\rho_w}{12}\int_0^\infty D^3 N(D) w_t^3(D) dD \qquad (5)$$

where ρ_w is the water density (kg/m^3). The second curve of Fig. 1 is obtained by computing eqn. 5 against R, and using eqn. 2.

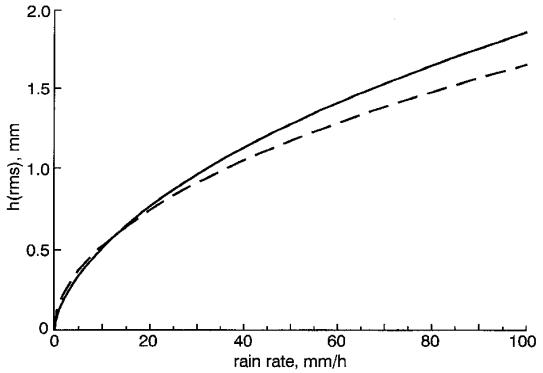

Fig. 1 *Rainfall rate against rms height of the water surface roughness*
——— Marshall–Palmer DSD model
– – – – rainfall with constant diameter raindrops

It is reasonably believed that the above simplifying assumptions hold for not too high rainfall rates; in any case, in the following we suppose eqn. 4 to be approximately valid up to 100mm/h. The two curves of Fig. 1 do not differ much from each other, indicating that the relationship obtained is not very sensitive to the adopted DSD. This feature is desirable, since it makes the modelling approach robust with respect to the DSD model.

2.2 Spatial wave spectrum

As shown in [1] and [4], the short-term transient (crowns and stalks) that follows the impulsive inputs due to falling drops does not affect the radar cross section at incidence angles close to nadir, but only the long-term transient (ring-waves) is relevant. Thus, we adopted the ring-wave frequency spectrum described in [5], converting it to the ring-wave wavenumber spectrum. Under the hypothesis that the ring-wave phenomenon is independent of the angular direction (azimuth-symmetric surface), such spectra can be expressed in terms of the radial wavenumber spectrum

(RWS), as shown in the following Section. As suggested in [5], the dependence of the RWS on rainfall intensity can indeed be approximated as follows:

$$S_R(K) = \langle h^2 \rangle S(K) \tag{6}$$

where $S(K)$ is the RWS normalised with respect to $\langle h^2 \rangle$. $S(K)$ is defined by $S(K)dK = \hat{\varphi}(\omega)d\omega$ and by the appropriate capillary–gravity wave dispersion formula [17, 18], where $\hat{\varphi}(\omega)$ is the normalised folded frequency spectrum given in [5] (defined for $\omega > 0$)

$$\hat{\varphi}(\omega) = \varphi_o \exp\left[-\pi\left(\frac{\ln(\omega/2\pi f_p)}{\Delta f/f_p}\right)^2\right] \tag{7}$$

where $f_p \approx 6$Hz, $\Delta f \approx 5$Hz and φ_o depends on R. Fig. 2 (after [5]) shows how such a log-Gaussian model fits the aforementioned experimental data relative to a normalised frequency spectrum.

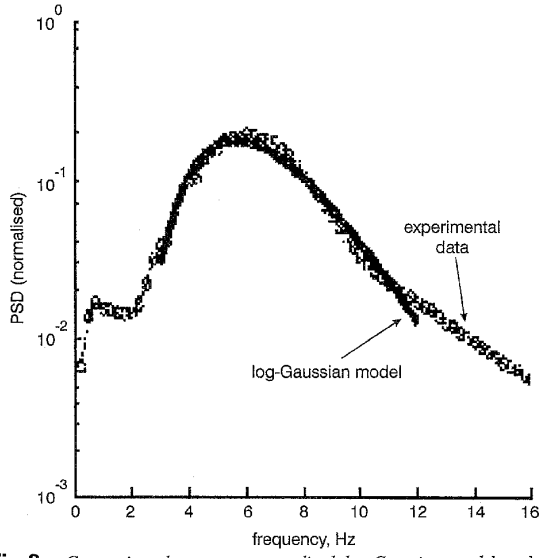

Fig. 2 *Comparison between a normalised log-Gaussian model and an experimentally determined frequency spectrum of artificial rain (after [5])*

3 Surface electromagnetic model

Here we report, for ease of reference, the basic expressions of the adopted EM model, based on the FWM for the backscatter case, described in detail in [6, 7], utilising the same original notation. The two-dimensional surface spectrum for an azimuth-symmetric surface, disregarding a normalisation factor, can be expressed as [17, 18]

$$W_B(K) = \frac{1}{K}S(K) \tag{8}$$

where $W_B(K)$ is the two-dimensional spectrum to be used in the FWM. If the mean square slope σ_{sl}^2 of the rough surface is small, say $\sigma_{sl}^2 < 0.2$, the effects of height–slope correlation can be neglected [19]; σ_{sl}^2 is then calculated as in [6, 19], and for ring-waves corrugation with spectrum $W_B(K)$ we obtained $\sigma_{sl}^2 = 3.34 \times 10^{-2}\langle h^2 \rangle$. Thus, condition $\sigma_{sl}^2 < 0.2$ is met for all values of $\langle h^2 \rangle$ considered in the following Section. Under this hypothesis, the unified FWM expressions of the like- and cross-polarised backscattering cross sections σ^{pq} become [6, 19, 20]

$$\sigma^{pq} = I^{pq}(\bar{\mathbf{n}}^f, \bar{\mathbf{n}}^i)Q(\bar{\mathbf{n}}^f, \bar{\mathbf{n}}^i) \tag{9}$$

where p and q stand for the scattered and incident wave polarisations (V or H), respectively. Furthermore

$$I^{pq}(\bar{\mathbf{n}}^f, \bar{\mathbf{n}}^i) = \iint A^{pq}(\bar{\mathbf{n}}^f, \bar{\mathbf{n}}^i, \bar{\mathbf{n}})p(h_x, h_z)dh_x dh_z \tag{10}$$

where

$$A^{pq}(\bar{\mathbf{n}}^f, \bar{\mathbf{n}}^i, \bar{\mathbf{n}}) = \frac{k^2}{\pi}\left|\frac{D^{pq}(\bar{\mathbf{n}}^f, \bar{\mathbf{n}}^i, \bar{\mathbf{n}})}{v_y(\bar{\mathbf{n}} \cdot \bar{\mathbf{a}}_y)}\right|^2 \tag{11}$$

and

$$Q(\bar{\mathbf{n}}^f, \bar{\mathbf{n}}^i) = 2\pi v_y^2 \int_0^\infty (\chi_2(v_y, -v_y) - |\chi(v_y)|^2)J_0(v_{xz}r_d)dr_d \tag{12}$$

are defined as in [6]. Expressions for the coefficients D^{pq} in eqn. 11 are reported in the Appendix. In the backscattering case, $\bar{\mathbf{v}} = v_x\bar{\mathbf{a}}_x + v_z\bar{\mathbf{a}}_z + v_y\bar{\mathbf{a}}_y = 2k\bar{\mathbf{n}}^f$, where k is the free space wavenumber of the EM wave [21], and $\bar{\mathbf{n}}^i = -\bar{\mathbf{n}}^f$, where $\bar{\mathbf{n}}^f = -\sin\vartheta \cdot \bar{\mathbf{a}}_x + \cos\vartheta \cdot \bar{\mathbf{a}}_y$ is the unit vector pointing from the surface towards the radar; the unit vectors $\bar{\mathbf{a}}_x$, $\bar{\mathbf{a}}_x$ are, respectively, parallel and perpendicular to the plane of the surface and ϑ is the incidence angle. Eqn. 12 reports the $Q(\bar{\mathbf{n}}^f, \bar{\mathbf{n}}^i)$ function explicitly valid for the azimuthal symmetry case; it involves the Bessel function of zero order J_o, where $v_{xz}^2 = v_x^2 + v_z^2$ is the transverse component of $\bar{\mathbf{v}}$. The unit vector $\bar{\mathbf{n}}$, locally perpendicular to the surface, is a function of the surface slopes h_x, h_z along the x, z directions, and $p(h_x, h_z)$ is the slopes probability density function (PDF), assumed Gaussian with variance σ_{sl}^2 [7, 21], calculated as in [6, 19].

The characteristic function (CF) and the joint characteristic functions (JCF) of the surface height h, are evaluated assuming a Gaussian PDF; they are, respectively [6]

$$\chi(v_y) = \exp(-v_y^2\langle h^2 \rangle/2)$$
$$\chi_2(v_y, -v_y) = \exp(-v_y^2\langle h^2 \rangle + v_y^2\langle hh' \rangle) \tag{13}$$

where $\langle h^2 \rangle$ is the mean square surface height, and $\langle hh' \rangle = \langle h^2 \rangle \rho(r_d)$ is the azimuth-symmetric surface autocorrelation function.

In our analysis, we disregard the shadow function considered in [6], since we refer only to incidence angles not too far from nadir and to a small rms surface slope. The correlation coefficient $\rho(r_d)$ is related to the normalised spectrum through [6, 19]

$$\rho(r_d) = 2\pi \int_0^\infty \frac{W_B(v_{xz})}{4} J_0(v_{xz}r_d)v_{xz}dv_{xz} \tag{14}$$

where $W_B(v_{xz})$ is the normalised wavenumber spectrum, defined as in [6].

4 Evaluation of the NRCS of the sea surface corrugated by rain only

We report here the NRCS computed through the FWM in the case of a sea surface perturbed by rain only, for different values of frequency, incidence angle and rms height. Correspondingly, we also report the NRCS computed through the IEM. The purpose is to support and strengthen the cited experimental results in [1] and [5] with some EM modelling effort. A good agreement between FWM and IEM, as that shown below, can indeed be interpreted as a cross-validation of their capability of predicting the radar backscatter, accounting for rain effects.

Concerning the IEM, since a complete study about its range of validity has not been carried out for dielectric surfaces, we considered one of the most restrictive conditions, namely a Gaussian correlation function [12]. Thus, if L is the correlation length, we required $(kh(rms)) \cdot (kL) < 1.2\sqrt{\varepsilon_r}$, which is certainly met by the adopted spectrum.

The results refer to 5.6 and 13.75GHz. The dielectric constant against frequency of the EM waves is in [22, 23]; we have $\varepsilon_r = 65 - j36$ and $\varepsilon_r = 43 - j40$ for 5.6 and 13.75GHz, respectively. In Figs. 3 and 4, the NRCS against incidence angle is plotted for both the copolar horizontal (HH) and vertical (VV) returns at 13.75GHz. Dots and lines refer to FWM and IEM, respectively. At all incidence angles the agreement is fairly good both for 1mm rms height (Fig. 3), and for 2mm rms height (Fig. 4). Near nadir (incidence angles close to 5–10°) the NRCS is lower, in agreement with the shape of the spatial wavenumber spectrum, namely decreasing for decreasing wavenumbers [5]. However, at K_u band the NRCS decreases when the incidence angle exceeds 5–10°, owing to the absence of high wavenumber components in the spectrum (see Fig. 2). Note also that, when sufficiently far from nadir, the VV response is larger than the HH.

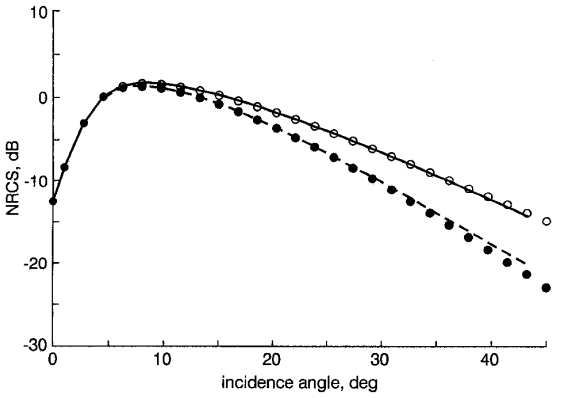

Fig. 3 *Sea surface NRCS (only rain corrugation) against incidence angle*
○ VV FWM
● HH FWM
——— VV IEM
- - - - HH IEM
f = 13.75GHz, $h(rms)$ = 1mm, $\varepsilon_r = 43 - j40$

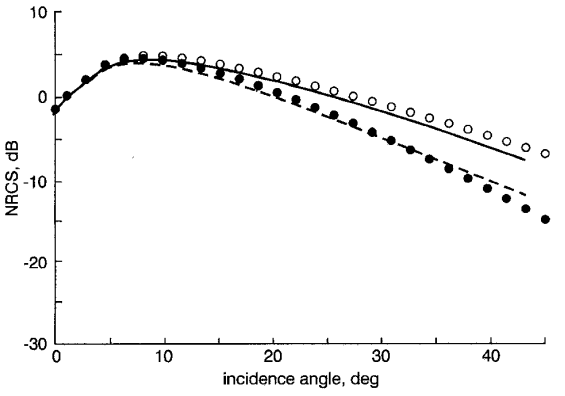

Fig. 4 *Sea surface NRCS (only rain corrugation) against incidence angle*
○ VV FWM
● HH FWM
——— VV IEM
- - - - HH IEM
f = 13.75GHz, $h(rms)$ = 2mm, $\varepsilon_r = 43 - j40$

In Figs. 5 and 6 the NRCS is plotted against rms height for both frequencies and for both HH and VV returns. The incidence angle is 10° in Fig. 5 and 30° in Fig. 6. $h(rms)$ ranges from 0.1–2.5mm, and the NRCS increases with it. The corresponding rainfall intensity can be obtained from Fig. 1. Similar results were obtained in the cited K_u band experiment at 30° incidence angle [1]. At both bands the same trend is observed, but at K_u band the NRCS is greater, being the EM wavelength closer to the rms height of the surface.

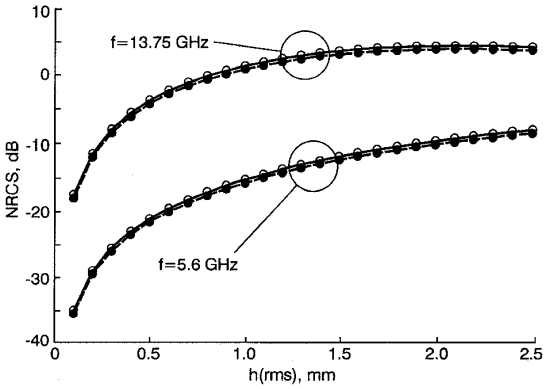

Fig. 5 *Sea surface NRCS (only rain corrugation) against rms height for both VV and HH responses at 5.6 and 13.75GHz, for an incidence angle of 10°*
○ VV FWM
● HH FWM
——— VV IEM
- - - - HH IEM

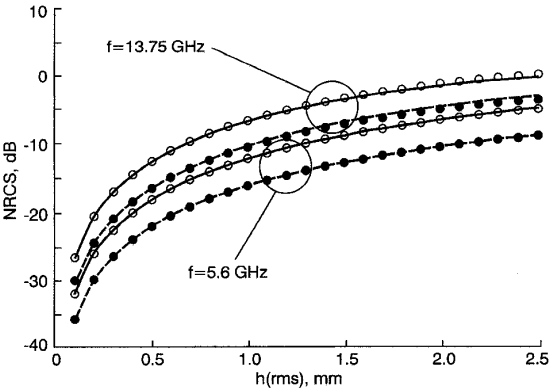

Fig. 6 *Sea surface NRCS (only rain corrugation) against rms height for both VV and HH responses at 5.6 and 13.75GHz, for an incidence angle of 30°*
○ VV FWM
● HH FWM
——— VV IEM
- - - - HH IEM

5 EM modelling of the sea surface corrugated by both wind and rain

The FWM was applied assuming that the surface roughness is the superposition of two statistically independent random processes h_R and h_W induced by rainfall and wind, respectively. This assumption is mainly based on the different scale of the two perturbations:

(*a*) Rain causes very local and non-coherent elementary perturbations on the sea surface. Their rms height is of the order of a few millimetres (see also Fig. 1).

(*b*) Wind is a wide-area source (often strongly coherent) of sea surface perturbations, including strong

stationary components. Wind roughness values reported by Apel [24] show that the standard deviation of the wind induced corrugation is much larger than that induced by rain.

(*c*) The wind- and rainfall-induced perturbations have quite different correlation lengths. These are some metres for wind [6, 24] and a few centimetres for rainfall [5].

(*d*) Statistically averaging the above effects over the sea surface illuminated by radar (in a stationary field), as implicit for cross-section evaluation, should improve conditions for the application of the followed approach. Therefore, besides independence, the following hypotheses were exploited:

(i) The large-scale process h_W is ridden by the small-scale process h_R, defined through a local reference system jointly with h_W. At a generic point of the surface, h_R is represented by a set of three orthogonal unit vectors that depend upon the local slope of the wind roughness h_W

(ii) The correlation length L_W of h_W is much larger than the correlation length L_R of h_R.

Exploiting such hypotheses, since $\sigma_{sl}^2 < 0.2$ for both surfaces, the CF and JCF are properly decomposed [7], and the NRCS expression changes from eqn. 9 to [25, 26]

$$\sigma^{pq} = \int_{\bar{\mathbf{n}}} A^{pq}(\bar{\mathbf{n}}^f, \bar{\mathbf{n}}^i, \bar{\mathbf{n}}) Q(\bar{\mathbf{n}}^f, \bar{\mathbf{n}}^i, \bar{\mathbf{n}}) p(\bar{\mathbf{n}}) d\bar{\mathbf{n}} \quad (15)$$

where

$$Q(\bar{\mathbf{n}}^f, \bar{\mathbf{n}}^i, \bar{\mathbf{n}}) = |\chi^R(\bar{\mathbf{v}} \cdot \bar{\mathbf{n}})|^2 Q_W(\bar{\mathbf{n}}^f, \bar{\mathbf{n}}^i) + (\bar{\mathbf{n}} \cdot \bar{\mathbf{a}}_y) Q_R(\bar{\mathbf{n}}^f, \bar{\mathbf{n}}^i, \bar{\mathbf{n}}) \quad (16)$$

Q_W and Q_R depend on the statistics of the phase of the EM wave, as determined by the height distribution of the rough surface relevant to wind and rain, respectively. Q_W is given by eqn. 12, substituting the wind surface height h_W in eqn. 13. We state in advance that, as specified in Section 5.1, we considered an azimuth-symmetric approximation of the sea surface wind corrugation spectrum. In fact, examining the NRCS data reported by Schroeder *et al.* [15], for incidence angles ranging from 0–60° and different wind velocities, it can be noticed that the difference between up-, down- and cross-wind measurements becomes remarkable only for angles larger than 20°. Thus, for incidence angles close to nadir the natural asymmetry of the wind-induced corrugation can be neglected. For Q_R we have instead

$$Q_R(\bar{\mathbf{n}}^f, \bar{\mathbf{n}}^i, \bar{\mathbf{n}}) = 2\pi v_y^2 \int_0^\infty (\chi_2^R(\bar{\mathbf{v}} \cdot \bar{\mathbf{n}}, -\bar{\mathbf{v}} \cdot \bar{\mathbf{n}}) - |\chi^R(\bar{\mathbf{v}} \cdot \bar{\mathbf{n}})|^2) \times J_0(v_{wxz} r_{wd}) r_{wd} dr_{wd} \quad (17)$$

where the CF and JCF are now calculated by means of the height distribution h_R with respect to the local vector $\bar{\mathbf{n}}$ normal to h_W (and not with respect to a_y as in eqn. 12). The integration variable r_{wd} is also the argument of the correlation function appearing in the JCF of eqn. 17; the subscript w recalls that it rides h_W. The term $v_{wxz} = \sqrt{[|\bar{\mathbf{v}}|^2 - |\bar{\mathbf{v}} \cdot \bar{\mathbf{n}}|^2]}$ is the projection of $\bar{\mathbf{v}}$ on the local plane tangent to h_W [7]. The result is averaged over the slopes of the large-scale process. Note that $Q_R(\bar{\mathbf{n}}^f, \bar{\mathbf{n}}^i, \bar{\mathbf{n}})$ is weighted by the slope of the large-scale surface while Q_W is not, as a consequence of the fact that h_R rides h_W. This corresponds to computing the ring-waves contribution through a statistical average over the slopes of the wind-roughened surface. Also in this case, shadowing effects were not accounted for.

Finally, notice that the EM model requires the height standard deviation $h_R(rms)$ of the small-scale process h_R, that can be related to the rain rate R through the curves of Fig. 1.

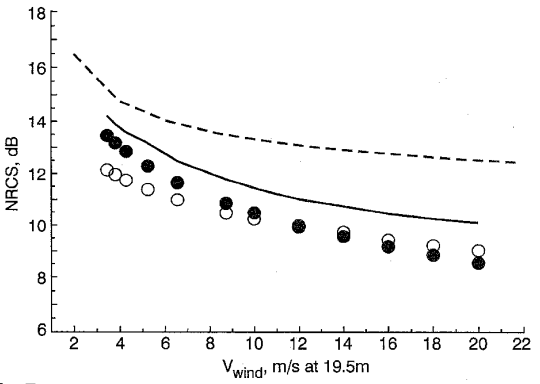

Fig. 7 *Sea surface NRCS (only wind corrugation) against wind velocity for nadir incidence*
Comparison between experimental data and the results obtained using models based on an approximated Pierson–Moscowitz spectrum and on an Apel spectrum
f = 13.75GHz, nadir incidence
○ AAFE RADSCAT (1)
● AAFE RADSCAT (2)
---- FWM (approximated Pierson–Moskowitz)
——— FWM (Apel)

5.1 Evaluation of the NRCS of the sea surface corrugated by wind and rainfall at nadir incidence

As mentioned in Section 1, nadir incidence experimental NRCS data for a sea surface perturbed by both wind and rain are not available in the literature. However, a partial evaluation of the applicability of the described FWM-based model was possible, by comparing its predictions with experimental data obtained by Schroeder *et al.* at 13.9GHz in the case of a sea surface perturbed by wind only [15]. Fig. 7 reports such a comparison. Measurement values (dots) were taken from the regression line in [15] and were made in two distinct experiments; the two curves represent two predictions based on the approximated Pierson–Moskowitz spectrum [6, 27] and on the spectrum reported by Apel in [24]. In particular, when using the latter, the azimuth dependence was averaged to deal with an azimuth-symmetric spectrum consistent with the assumptions made in this paper. As expected, the Apel spectrum fits the actual NRCS behaviour better than the approximated Pierson–Moskowitz spectrum, even if the predicted NRCS is slightly larger. Schroeder *et al.* [15] indeed noted a similar discrepancy by comparing their measurements with the SASS I model. However, the difference is of the order of the uncertainty of the measurements, and may also be attributed to the Apel spectrum. The approximated Pierson–Moskowitz spectrum is not accurate for nadir incidence, but we found that its predictions off nadir are in rather good agreement with the experimental results.

Our general theoretical results are finally summarised in Fig. 8, that reports the sea surface NRCS against rainfall rate R at 13.9GHz, for some wind velocities and nadir incidence obtained using the FWM-based model and the Apel spectrum [24]. We point out that

the NRCS variations due to rainfall rate are of the same order of magnitude as those due to wind velocity. This justifies the inclusion of rainfall-induced corrugation in the EM model. In fact, trying to predict sea NRCS without accounting for rainfall corrugation may easily lead to bias errors comparable with those that may be caused by an incorrect choice of the wind spectrum.

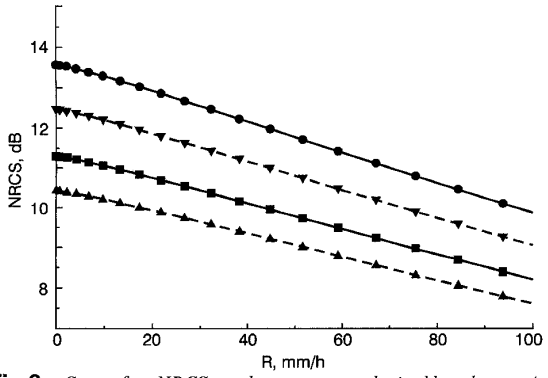

Fig. 8 *Sea surface NRCS copolar component, obtained based on an Apel spectrum, against rainfall rate R for various wind velocities*
f = 13.75GHz, nadir incidence
—●— v_w = 4.3m/s
—▼— v_w = 6.6m/s
—■— v_w = 10.6m/s
—▲— v_w = 16.0m/s

6 Conclusions

The characterisation of the NRCS of the sea surface, when perturbed by rainfall only and by the joint action of wind and rainfail was the main objective of this paper. An EM model has been considered, based on the FWM theory.

To analyse phenomena related to rainfall-induced variations of NRCS, it was necessary to derive a relationship between the rainfall intensity and the rms height of the sea surface, this result is not available in the literature for natural rain. By exploiting results referring to an artificial rainfall experiment and energetic considerations, we obtained an approximate theoretical relationship for two different DSD models.

Considering rainfall-induced corrugation only, the FWM NRCS was compared with the IEM NRCS, and a very good agreement was shown at 5.6 and 13.75GHz. Incidentally, this can be considered as a confirmation of the consistency of both models with respect to the problem examined. Typically expected NRCS behaviour has been highlighted or confirmed; near nadir, the predicted echo is smaller than at greater incidence angles, and it increases as the surface rms height increases. It has been shown that in the case of sea surface perturbed by rainfall-induced ring-waves, the VV response is larger than the HH, at both C and K_u bands, and that such a difference increases with increasing incidence angle. Moreover, the NRCS is always larger at K_u band than at C band. As a complementary analysis, the predicted NRCS by the FWM for the sea surface corrugated by only wind has been compared with experimental data, with rather good results. Finally, the case of induced corrugation by the joint action of wind and rain has been considered, showing that additional roughness induced by rainfall cannot be considered as a side issue in the backscatter mechanisms at the K_u band. Actually, experiments would be needed to determine errors due to the EM model assumptions made in Section 5, as well as possible limitations associated with the use of high-frequency bands. Indeed, major model limitations are expected to be related to strong and/or nonstationary winds.

All the results summarised above were obtained disregarding the surface damping effects, typically induced by heavy rainfall, that cause an increase of NRCS at nadir incidence [28, 29]. This problem, requiring a quite complex physical analysis and EM characterisation, is worth further investigation, necessarily supported by experimental measurements. At the K_u band it is however expected that, even when damping effects occur, ring-waves should play a dominant role since their size is comparable with the EM wavelength. This seems to be confirmed by the analysis of TOPEX/Poseidon altimeter data [30].

The proposed EM model is exploitable by algorithms devoted to rainfall retrieval over the sea surface, as discussed in the companion paper [2]. Its use for revealing features (also polarimetric) and for separating sea surface radar return from volumetric rainfall return is foreseeable. Also, it could be exploited in scatterometry to improve/evaluate performance of algorithms for wind speed computation, to highlight the bias effects due to rain roughness, or in altimetry to predict effects of rainfall (e.g. to estimate K_u band attenuation by atmospheric liquid water, as suggested in [30]).

7 Acknowledgments

This work has been supported by the Italian Ministry of University and Technological Research and by the Italian Space Agency. The authors would also like to thank Prof. P. Sobieski for useful discussions, and an anonymous reviewer for comments.

8 References

1 BLIVEN, L.F., BRANGER, H., SOBIESKI, P.W., and GIOVANANGELI, J.P.: 'An analysis of scatterometer returns from a water surface agitated by artificial rain: evidence that ring-waves are the main feature', *Int. J. Remote Sens.*, 1993, **14**, (12), pp. 2315–2329
2 CAPOLINO, F., FACHERIS, L., GIULI, D., and SOTTILI, F.: 'Rainfall profile retrieval through spaceborne rain radars utilising a sea surface NRCS model', *IEE Proc. Radar, Sonar Navig.*, 1998, **145**, (4), pp. 233–239
3 WETZEL, L.B.: 'On the theory of electromagnetic scattering from a raindrop splash', *Radio Sci.*, 1990, **25**, (6), pp. 1183–1197
4 SOBIESKI, P.W., and BLIVEN, L.F.: 'Scatterometry of a drop impact on a salt water surface', *Int. J. Remote Sens.*, 1995, **16**, (14), pp. 2721–2726
5 BLIVEN, L.F., SOBIESKI, P.W., and ELFOUHAILY, T.: 'Ring-wave frequency spectra: measurements and model'. Proceedings of IGARSS'95, Florence, Italy, July 1995, pp. 830
6 BAHAR, E., and FITZWATER, M.A.: 'Scattering cross section for composite rough surfaces using the unified full wave approach', *IEEE Trans.*, 1984, **AP–32**, (7), pp. 730–734
7 BAHAR, E.: 'Review of the full wave solutions for rough surface scattering and depolarization: comparisons with geometric and physical optics, perturbation, and two-scale hybrid solution', *J. Geophys. Res.*, 1987, **92**, (C5), pp. 5209–5224
8 THORSOS, E.I., and WINEBRENNER, D.P.: 'An examination of the full-wave method for rough surface scattering in the case of small roughness', *J. Geophys. Res.*, 1991, **96**, (C9), pp. 17107–17121
9 BAHAR, E.: 'Examination of full-wave solutions and "exact numerical results" for one-dimensional slightly rough surface', *J. Geophys. Res.*, 1991, **96**, (C9), pp. 17123–17131
10 COLLIN, R.E.: 'Electromagnetic scattering from perfectly conducting rough surfaces (a new full wave method)', *IEEE Trans. Antennas Propag.*, 1992, **40**, (12), pp. 1466–1477
11 COLLIN, R.E.: 'Full wave theories for rough surface scattering: an updated assessment', *Radio Sci.*, **29**, (5), pp. 1237–1254
12 FUNG, A.K.: 'Microwave scattering and emission models and their applications' (Artech House Inc., 1994)

13 FUNG, A.K., and CHEN, K.S.: 'A validation of the IEM surface scattering model'. Proceedings of IGARSS'95, Florence, Italy, July 1995, pp. 933–935
14 CHEN, K.S., and FUNG, A.K.: 'A comparison of backscattering models for rough surfaces', *IEEE Trans. Geosci. Remote Sens.*, 1995, **33**, (1), pp. 195–200
15 SCHROEDER, L.C., SCHAFFNER, P.R., MITCHELL, J.L., and JONES, W.L.: 'AAFE RADSCAT 13.9-GHz measurements and analysis: wind-speed signature of the ocean', *IEEE J. Ocean. Eng.*, 1985, **10**, pp. 346–357
16 DOVIAK, R.J., and ZRNIC', D.S.: 'Doppler radar and weather observations' (Academic Press Inc., 1992), 2nd edn
17 GUISSARD, A., BAUFAYS, C., and SOBIESKI, P.W.: 'Sea surface description requirements for electromagnetic scattering calculations', *J. Geophys. Res.*, 1986, **91**, (C2), pp. 2477–2492
18 GUISSARD, A., BAUFAYS, C., and SOBIESKI, P.W.: 'Fully and nonfully developed sea models for microwave remote sensing applications', *Remote Sens. Environ.*, 1994, **48**, pp. 25–38
19 BAHAR, E., and KUBIK, R.D.: 'Tilt modulation of high resolution radar backscatter cross sections: unified full wave approach', *IEEE Trans. Geosci. Remote Sens.*, 1993, **31**, (6), pp. 1229–1242
20 BAHAR, E., and LEE, B.S.: 'Full wave solutions for rough-surface bistatic radar cross sections: comparison with small-perturbation, physical optics, numerical, and experimental results', *Radio Sci.*, 1994, **29**, (2), pp. 407–429
21 BAHAR, E., BARRICK, D.E., and FITZWATER, M.A.: 'Computations of scattering cross sections for composite surfaces and the specification of the wavenumber where spectral splitting occurs', *IEEE Trans.*, 1983, **AP–31**, (5), pp. 698–709
22 STOGRYN, A.: 'Equation for calculating the dielectric constant of saline water', *IEEE Trans.*, 1971, **MTT–19**, pp. 733–736
23 ULABY, F.T., MOORE, R.K., and FUNG, A.K.: 'Microwave remote sensing, active and passive' (Artech House Inc., 1986), Vol. III
24 APEL, J.R.: 'An improved model of the ocean surface wave vector spectrum and its effects on radar backscattering', *J. Geophys. Res.*, 1994, **99**, (C8), pp. 16,269-16,291
25 CAPOLINO, F., FACHERIS, L., GIULI, D., and SOTTILI, F.: 'Estimating RCS of the sea surface perturbed by rain for rainfall rate retrieval'. Proceedings of IGARSS'96, Lincoln, Nebraska, USA, May 1996
26 CAPOLINO, F., FACHERIS, L., GIULI, D., and SOTTILI, F.: 'The determination of the sea surface NRCS when corrugated by blowing wind and rainfall: an application to rainfall rate measurement over sea'. Proceedings of ICAP 97, Edinburgh, UK, April 1997, pp. 2.186–2.190
27 BROWN, G.S.: 'Backscattering from a Gaussian-distributed perfectly conducting rough surface', *IEEE Trans.*, 1978, **AP–26**, (3), pp. 472–482
28 ATLAS, D.: 'Footprints of storms on the sea: a view from spaceborne synthetic aperture radar', *J. Geophys. Res.*, 1994, **99**, pp. 7961–7969
29 DURDEN, S.L., HADDAD, Z.S., IM, E., KITIYAKARA, A., LI, F.K., TANNER, A.B., and WILSON, W.J.: 'Measurement of rainfall path attenuation near nadir: a comparison of radar and radiometer methods at 13.8 GHz', *Radio Sci.*, 1995, **30**, (4), pp. 943–947
30 TOURNADRE, J., and MORLAND, J.C.: 'The effects of rain on TOPEX/Poseidon altimeter data', *IEEE Trans. Geosci. Remote Sens.*, 1997, **35**, (5), pp. 1117–1135

9 Appendix

We report here the expressions of the terms involved in the FWM for the backscatter case. Posing $\bar{\mathbf{n}}^i = -\bar{\mathbf{n}}^f$, the terms D^{pq} in eqn. 11 are given by

$$\overline{\overline{\mathbf{D}}} = \begin{pmatrix} D^{VV} & D^{VH} \\ D^{HV} & D^{HH} \end{pmatrix} = (-\bar{\mathbf{n}} \cdot \bar{\mathbf{n}})\overline{\overline{\mathbf{T}}}^f \overline{\overline{F}}\,\overline{\overline{T}}^i \tag{18}$$

The matrix $\overline{\overline{\mathbf{F}}}$ involves reflection coefficients in the local reference system [7]. Assuming the magnetic permeability $\mu_r = 1$

$$\overline{\overline{\mathbf{F}}} = \begin{pmatrix} F^{VV} & F^{VH} \\ F^{HV} & F^{HH} \end{pmatrix} \tag{19}$$

where

$$\begin{aligned} F^{VV} &= \frac{(1-\varepsilon_r)(s_0^2 + c_1^2)}{(\sqrt{\varepsilon_r}c_0 + c_1)^2} \\ F^{HH} &= \frac{\varepsilon_r - 1}{(c_0 + \sqrt{\varepsilon_r}c_1)^2} \\ F^{HV} &= F^{VH} = 0 \end{aligned} \tag{20}$$

in which S_0, C_0 (real), S_1 and C_1 (complex) are sine and cosine of incident and transmitted field angles, accounting for the complex relative dielectric constant ε_r

$$\begin{aligned} C_0 &= \bar{\mathbf{n}}^f \cdot \bar{\mathbf{n}} \qquad S_0 = \sqrt{1 - C_0^2} \\ S_1 &= \frac{1}{\sqrt{\varepsilon_r}} S_0 \qquad C_1 = \sqrt{1 - S_1^2} \end{aligned} \tag{21}$$

The matrices $\overline{\overline{\mathbf{T}}}^f$, $\overline{\overline{\mathbf{T}}}^i$, accounting for the change of the co-ordinate system (central to local), coincide in the backscatter case [7]

$$\overline{\overline{\mathbf{T}}}^f = \begin{pmatrix} c_\psi^f & -s_\psi^f \\ s_\psi^f & c_\psi^f \end{pmatrix} \tag{22}$$

$$\begin{aligned} c_\psi^f &= \frac{(\bar{\mathbf{n}}^f \times \bar{\mathbf{a}}_y) \cdot (\bar{\mathbf{n}}^f \times \bar{\mathbf{n}})}{|\bar{\mathbf{n}}^f \times \bar{\mathbf{a}}_y||\bar{\mathbf{n}}^f \times \bar{\mathbf{n}}|} \\ s_\psi^f &= \frac{(\bar{\mathbf{n}}^f \times \bar{\mathbf{a}}_y) \times (\bar{\mathbf{n}}^f \times \bar{\mathbf{n}})}{|\bar{\mathbf{n}}^f \times \bar{\mathbf{a}}_y||\bar{\mathbf{n}}^f \times \bar{\mathbf{n}}|} \cdot \bar{\mathbf{n}}^f \end{aligned} \tag{23}$$